energies

MDPI

Article

A 36-Pulse Diode Rectifier with an Unconventional Interphase Reactor

Yuxin Lian , **Shiyan Yang**, **Hongqi Ben** and **Wei Yang** *

School of Electrical Engineering and Automation, Harbin Institute of Technology, Harbin 150001, China; lianyx@hit.edu.cn (Y.L.); syyang@hit.edu.cn (S.Y.); benhq@hit.edu.cn (H.B.)

* Correspondence: yangv@hit.edu.cn; Tel.: +86-451-8641-3604

Received: 19 January 2019; Accepted: 24 February 2019; Published: 1 March 2019

check for updates

Abstract: This paper proposes a simple 36-pulse diode rectifier with an unconventional interphase reactor (IPR) and single-phase full-wave rectifier (SFR). The primary winding of the unconventional IPR is double tapped and the secondary winding is connected with SFR. The operation mode of the unconventional IPR is analyzed, and the optimal tap ratio and turn ratio of the unconventional IPR are designed from both viewpoints of input line current and load voltage. With the optimal parameters of the unconventional IPR, the proposed rectifier extends the conventional 24-pulse rectifier operation to 36-pulse operation and draws near sinusoidal input line currents, the total harmonic distortion (THD) of which is about 5.035%. The kVA rating of the unconventional IPR is about 2.6% of the output power. Compared with the conventional 36-pulse rectifier with triple-tapped IPR, the proposed 36-pulse rectifier is easy and simple to implement instead of using control circuits. Experiment results are provided to verify the theoretical analysis.

Keywords: interphase reactor (IPR); 36-pulse rectifier; total harmonic distortion (THD); harmonic reduction

---

1. Introduction

The multipulse rectifier (MPR) technique is one of the most important and commonly used methods in electrochemical, high-voltage dc transmission, aircraft converter systems, plasma torches, and so on [1–3]. MPRs are fed from a three-phase utility resulting in a higher total harmonic distortion (THD) and other power quality problems. Modern MPRs are expected to draw sinusoidal input current form the utility [4]. The MPR pulse number determines the harmonic reduction ability [5], therefore, increasing the pulse number is one of the most effective methods in MPR.

There are two common ways to increasing the pulse number, one is to augment the output phase number of phase-shift transformer, and the other way is to install the auxiliary harmonic reduction circuit at the dc or ac side of the MPR. Presently, the use of 6-pulse/12-pulse MPR-based phase-shift transformers in industrial applications exhibits high THD. Several MPRs with phase-shift transformers are proposed through various phase-shift transformer connections to increase the output number of the phase-shift transformer [6–9]. These MPR-based phase-shift transformers are of either isolated or non-isolated type with symmetric configurations. An increase in pulse number using an autoconnected transformer is achieved by augmenting the output phases with a suitable phase shift between the output and supply voltages [10,11]. However, with the increasing number of output windings in a phase-shift transformer, the phase-shifting transformer structure becomes complicated and the utilization ratio of turn coils is depressed, causing difficulties in design and manufacture. Because the 12-pulser rectifier is the simplest and the most popular MPR, several circuit topologies with active or passive auxiliary circuits are proposed to install at the dc or ac side of 12-pulse rectifier, which can effectively lower the input line current harmonics [12–22]. The harmonic reduction at the dc-side is carried out by injecting current through an interphase reactor (IPR) [12]. For achieving sinusoidal input current and regulated dc output voltage, a power factor correction circuit connected at the output of uncontrolled rectifiers is presented in [13]. Among the numerous novel auxiliary harmonic reduction circuits, using a multitapped IPR to replace the IPR is the most common approach in harmonic reduction [16–18]. When the double-tapped IPR is used, the rectifier can effectively eliminate (12k ± 1)th (k is odd number) harmonics, the theoretical THD of input line current is about 7.6%, and the output voltage is 24 pulses under ideal condition. If the tap number is 3, the MPR needs control circuits and behaves as a 36-pulse rectifier. Though increasing the tap number can improve the pulse number and harmonic reduction ability, the additional diodes or thyristors linked with the taps are in series with the load and the total currents through the additional diodes or thyristors are equal to the load current. The conduction losses of the diodes or thyristors are serious, especially in low-voltage and high-current applications. In [19], a novel 24-pulse rectifier is proposed, in which the proposed IPR is unconventional and different from the multi-tapped IPR. An auxiliary single-phase full-wave rectifier is installed with the secondary winding of the proposed IPR, and the primary winding is central tapped. This modification extends the conventional four-star 12-pulse operation to 24-pulse operation.

In this paper, a 36-pulse diode rectifier with simple circuit configuration and low diode conduction losses is proposed. It consists of a three-phase bridge parallel 12-pulse rectifier, an unconventional IPR, and secondary rectifier circuit. The primary winding of the unconventional IPR and two diodes constitute a conventional double-tapped IPR, which is the first harmonic reduction method. The secondary winding connects secondary rectifier circuit to formulate the second harmonic reduction method. The secondary rectifier circuit is either a single-phase full-wave rectifier (SFR) or a single-phase diode-bridge rectifier. When the unconventional IPR is designed optimally, the proposed 36-pulse rectifier operates normally and simultaneously increases the pulse number of the load voltage and step number of the input line current. The theoretical THD of input current is about 5.035%. Compared with other 36-pulse rectifiers, the proposed rectifier is totally passive components without control circuits, and the conduction losses of the secondary rectifier circuit are very low because of the output of secondary rectifier circuit is connected in parallel with the load. In application, the THD of input line current is less than 4% due to the leakage inductance of autotransformer and inductance of IPR.

2. Proposed 36-Pulse Rectifier with Unconventional IPR

Figure 1 shows the circuit configuration of the proposed 36-pulse diode rectifier. It consists of a delta-connected autotransformer, two three-phase diode-bridge rectifiers, a zero sequence blocking transformer (ZSBT), an unconventional IPR, and a SFR. The delta-connected autotransformer is used to be the phase-shifting transformer. Figure 2a shows the winding configuration of delta-connected autotransformer. Figure 2b shows the phasor diagram of delta-connected autotransformer.

The proposed 36-pulse diode rectifier contains two three-phase diode-bridge rectifiers, the phase-shifting angle of the phase-shift transformer should be $\pi/6$ from the viewpoint of eliminating 5th and 7th harmonics [22]. As discussed in [23], when the phase-shifting angle is $\pi/6$, the winding configuration of delta-connected autotransformer shown in Figure 2a is the simplest and the delta-connected autotransformer has the least kVA rating. Figure 2b shows the phasor diagram of delta-connected autotransformer. When the delta-connected autotransformer has the simplest winding configuration, the angle α is equal to half of the phase-shifting angle [24]. Therefore, as discussed in [24], the angle is equal to be $\pi/12$ and the winding turns of autotransformer in Figure 2 should satisfy:

$$\frac{N_1}{N_2} = \frac{\sqrt{3}}{2 - \sqrt{3}} \tag{1}$$

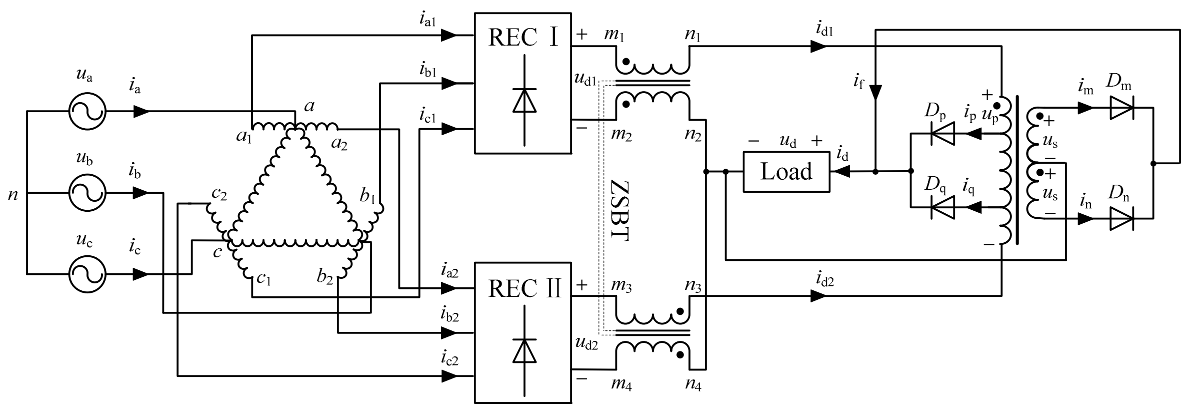

Figure 1. Schematic diagram of the proposed 36-pulse diode rectifier.

ZSBT can generate high impedance for three frequency multiplication current to ensure that three-phase diode-bridge rectifier operates independently with $2\pi/3$ conduction of each diode. Because of the delta-connected autotransformer is not isolated, the ZSBT is necessary. The ZSBT exhibits significant impedance for zero-sequence current components, thereby eliminating unwanted conduction sequence of the rectifier diodes in an autoconnected system [5]. As discussed in [5], with a properly designed ZSBT, the voltage across the ZSBT contains only triple frequency components and it impedes the flow of triple harmonic currents to ensure independent six-pulse operation of the two three-phase diode-bridge rectifiers REC I and II. The primary double-tapped winding of the unconventional IPR can absorb the instantaneous difference of the output voltage of the two three-phase diode-bridge rectifiers. The secondary windings of the unconventional IPR have a center tap to install SFR. The ac side of the SFR connects the secondary windings, and the dc side of SFR connects the load. When the double-tapped position and turn ratio of the unconventional IPR meet some condition, the proposed 36-pulse rectifier operates normally.

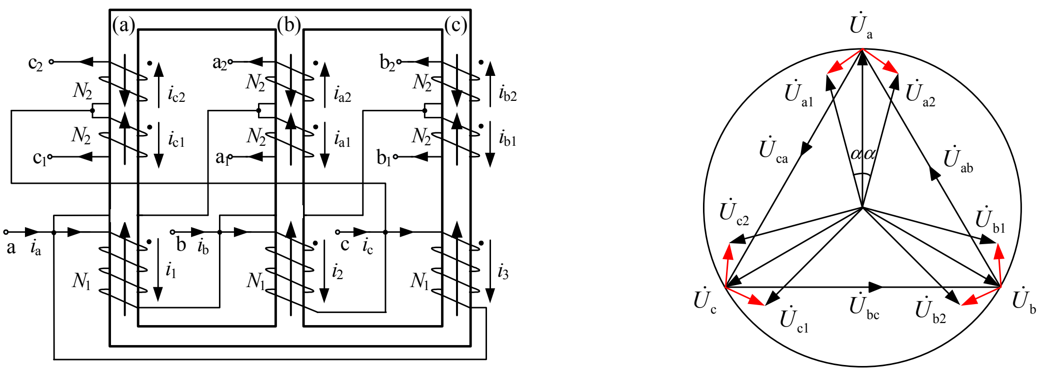

(**a**) (**b**)

Figure 2. (**a**) Winding configuration of the delta-connected autotransformer; (**b**) Phasor diagram of the delta-connected autotransformer.

Figure 3a,b show the tap structure and the winding configuration of the unconventional IPR. The tap ratio $\alpha_{\rm m}$ is defined as:

$$\alpha_{\rm m} = \frac{N_{\rm OT}}{N_{\rm P}} = \frac{N_{\rm OT'}}{N_{\rm P}} \tag{2}$$

The turn ratio of the primary and the half secondary windings of the unconventional IPR is:

$$\alpha_{\rm n} = \frac{N_{\rm S}}{N_{\rm P}} \tag{3}$$

where N_P and N_S are the numbers of turn of the primary and half secondary windings of the unconventional IPR, respectively.

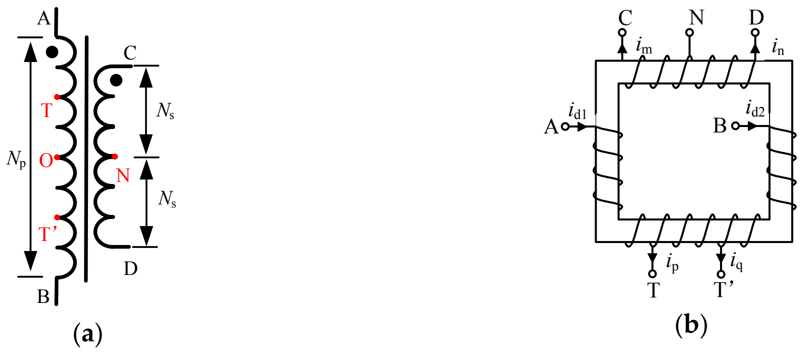

Figure 3. (**a**) Tap structure of the unconventional IPR; (**b**) Winding configuration of the unconventional IPR.

3. Operation Mode and Optimal Design of Unconventional IPR

3.1. Operation Mode

In order to demonstrate the operation mode of the unconventional IPR, the following assumptions are given below:

(1) The load of proposed rectifier is a large inductance loading and the load current i_d can be view as a constant Id.

(2) The leakage inductances and resistances of autotransformer and unconventional IPR are neglected.

(3) Assume that the input voltage of the proposed 36-pulse rectifier is:

$$\begin{cases} u_a = U_m \sin(\omega t) \\ u_b = U_m \sin(\omega t - 2\pi/3) \\ u_c = U_m \sin(\omega t + 2\pi/3) \end{cases} \tag{4}$$

where U_m is the amplitude of the input phase voltage, ω is the angular frequency of the input phase voltage.

(4) Assume that the voltage across the secondary winding of the unconventional IPR is u_s, and the load voltage is u_d. The output voltage of the two three-phase diode-bridge rectifiers is u_{d1} and u_{d2}, respectively.

The operation mode of the unconventional IPR is determined by the relation of u_s and u_d, and the relation of u_{d1} and u_{d2}. Therefore, there are four operation modes, as shown in Figure 4:

Mode I: When $|u_s| < u_d$ and $u_{d1} > u_{d2}$, the unconventional IPR operates under mode I, as shown in Figure 4a. In this mode, the diodes of the SFR are reverse-biased and OFF, the current i_f is equal to zero, and the SFR does not work. Diode D_p of the primary winding is forward-biased and ON, and diode D_q is reverse-biased and OFF. The unconventional IPR operates as a double-tapped IPR. The output currents of the two three-phase diode-bridge rectifiers are:

$$\begin{cases} i_{d1} = (0.5 + \alpha_m) I_d \\ i_{d2} = (0.5 - \alpha_m) I_d \end{cases} \tag{5}$$

The load voltage is:

$$u_d = \frac{(u_{d1} + u_{d2})}{2} + \alpha_m (u_{d1} - u_{d2}) \tag{6}$$

Mode II: When $|u_\mathrm{s}| < u_\mathrm{d}$ and $u_\mathrm{d1} < u_\mathrm{d2}$, the unconventional IPR operates under mode II, as shown in Figure 4b. In this mode, the diodes of the SFR are reverse-biased and OFF, the current i_f is equal to zero, and the SFR does not work. Diode D_q of the primary winding is forward-biased and ON, and diode D_p is reverse-biased and OFF. The unconventional IPR operates as a double-tapped IPR. The output currents of the two three-phase diode-bridge rectifiers are:

$$\begin{cases} i_\mathrm{d1} = (0.5 - \alpha_\mathrm{m}) I_\mathrm{d} \\ i_\mathrm{d2} = (0.5 + \alpha_\mathrm{m}) I_\mathrm{d} \end{cases} \tag{7}$$

The load voltage is:

$$u_\mathrm{d} = \frac{(u_\mathrm{d1} + u_\mathrm{d2})}{2} - \alpha_\mathrm{m}(u_\mathrm{d1} - u_\mathrm{d2}) \tag{8}$$

Mode III: When $u_\mathrm{s} > u_\mathrm{d}$ and $u_\mathrm{d1} > u_\mathrm{d2}$, the unconventional IPR operates under mode III, as shown in Figure 4c. In this mode, diode D_m is forward-biased and turned ON, current i_m is positive, and it is injected to the load. Diode D_n is reverse-biased and OFF. Simultaneously, diode D_p is ON and diode D_q is OFF. During this time interval, because the load voltage u_d is greater than the voltage u_d2, the current i_d2 is equal to zero.

The MMF relationship of the unconventional IPR for this mode is:

$$i_\mathrm{d1} \cdot (0.5 - \alpha_\mathrm{m}) \cdot N_\mathrm{P} = i_\mathrm{m} \cdot N_\mathrm{S} \tag{9}$$

According to Kirchhoff's current law (KCL), the relation among i_m, i_f, i_p and i_d is:

$$i_\mathrm{f} + i_\mathrm{p} = i_\mathrm{m} + i_\mathrm{d1} = i_\mathrm{d} \tag{10}$$

Substituting Equations (2), (3) and (9) into Equation (10), Equation (10) is transformed to:

$$\frac{(0.5 - \alpha_\mathrm{m})}{\alpha_\mathrm{n}} \cdot i_\mathrm{d1} + i_\mathrm{d1} = i_\mathrm{d} \tag{11}$$

From Equations (9)–(11), the currents i_d1 and i_f are obtained as:

$$\begin{cases} i_\mathrm{d1} = \frac{\alpha_\mathrm{n}}{0.5 - \alpha_\mathrm{m} + \alpha_\mathrm{n}} I_\mathrm{d} \\ i_\mathrm{f} = \frac{0.5 - \alpha_\mathrm{m}}{0.5 - \alpha_\mathrm{m} + \alpha_\mathrm{n}} I_\mathrm{d} \end{cases} \tag{12}$$

According to Kirchhoff's voltage law (KVL), the voltage u_d1 and u_d2 meet:

$$\begin{cases} u_\mathrm{d1} - (0.5 - \alpha_\mathrm{m}) \frac{N_\mathrm{p}}{N_\mathrm{s}} u_\mathrm{d} = u_\mathrm{d} \\ u_\mathrm{d1} - \frac{N_\mathrm{p}}{N_\mathrm{s}} u_\mathrm{d} = u_\mathrm{d2} \end{cases} \tag{13}$$

Substituting Equation (3) into Equation (13) yields:

$$\begin{cases} u_\mathrm{d} = \frac{\alpha_\mathrm{n}}{0.5 - \alpha_\mathrm{m} + \alpha_\mathrm{n}} u_\mathrm{d1} \\ u_\mathrm{d2} = \frac{\alpha_\mathrm{n} - \alpha_\mathrm{m} - 0.5}{0.5 - \alpha_\mathrm{m} + \alpha_\mathrm{n}} u_\mathrm{d1} \end{cases} \tag{14}$$

Mode IV: When $-u_\mathrm{s} > u_\mathrm{d}$ and $u_\mathrm{d1} < u_\mathrm{d2}$, the unconventional IPR operates under mode IV, as shown in Figure 4d. In this mode, diode D_n is forward-biased and turned ON, current i_n is positive, and it is injected to the load. Diode D_m is reverse-biased and OFF. Simultaneously, diode D_q is ON and diode D_p is OFF. During this time interval, because the load voltage u_d is greater than the voltage u_d1, the current i_d1 is equal to zero.

The MMF relationship of the unconventional IPR for this mode is:

$$i_\mathrm{d2} \cdot (0.5 - \alpha_\mathrm{m}) \cdot N_\mathrm{P} = i_\mathrm{n} \cdot N_\mathrm{S} \tag{15}$$

The analysis is similar as the mode III, the currents i_{d2} and i_{f} are obtained as:

$$\begin{cases} i_{\mathrm{d2}} = \frac{\alpha_{\mathrm{n}}}{0.5-\alpha_{\mathrm{m}}+\alpha_{\mathrm{n}}} I_{\mathrm{d}} \\ i_{\mathrm{f}} = \frac{0.5-\alpha_{\mathrm{m}}}{0.5-\alpha_{\mathrm{m}}+\alpha_{\mathrm{n}}} I_{\mathrm{d}} \end{cases} \tag{16}$$

The voltage u_{d} and u_{d1} are obtained as:

$$\begin{cases} u_{\mathrm{d}} = \frac{\alpha_{\mathrm{n}}}{0.5-\alpha_{\mathrm{m}}+\alpha_{\mathrm{n}}} u_{\mathrm{d2}} \\ u_{\mathrm{d1}} = \frac{\alpha_{\mathrm{n}}-\alpha_{\mathrm{m}}-0.5}{0.5-\alpha_{\mathrm{m}}+\alpha_{\mathrm{n}}} u_{\mathrm{d2}} \end{cases} \tag{17}$$

From the above analysis, it is noted that the output currents i_{d1} and i_{d2} of the two three-phase diode-bridge rectifiers under operation modes III and IV are different from that of under operation modes I and II because of the SFR output current. When the parameters α_{m} and α_{n} of the unconventional IPR meet some conditions, the proposed MPR operates as a 36-pulse rectifier and reduces the harmonic in the input line current effectively.

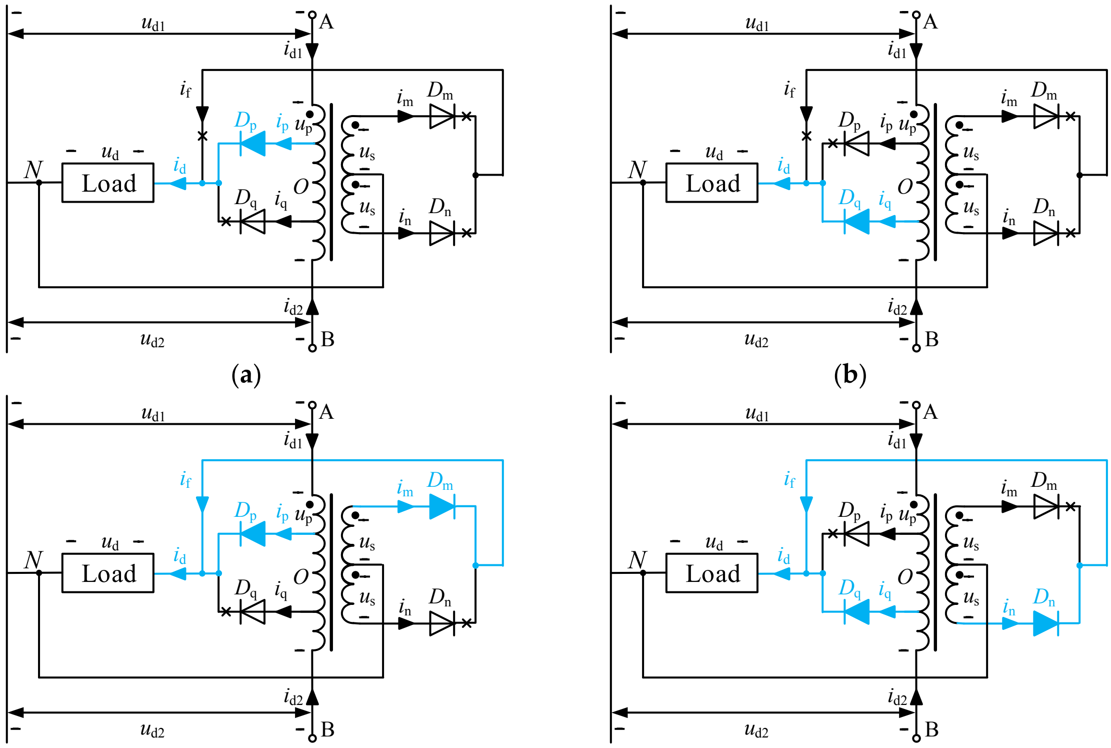

Figure 4. Operation modes of the unconventional IPR. (**a**) Operation mode I; (**b**) Operation mode II; (**c**) Operation mode III; (**d**) Operation mode IV.

3.2. Necessary Condition

According to the operation mode, if the maximum value of the voltage u_{s} is less than the minimum value of load voltage u_{d}, the unconventional IPR operates as double-tapped IPR and the MPR operates as 24-pulse rectifier. In order to make the unconventional IPR operate normally, the following necessary condition should meet:

$$|u_{\mathrm{s}}|_{\max} < u_{\mathrm{d\ min}} \tag{18}$$

From Figure 2a,b, the output voltages of the delta-connected autotransformer can be expressed as:

$$\begin{cases} u_{a1} = \sqrt{2}\left(\sqrt{3}-1\right)U_m \sin(\omega t + \pi/12) \\ u_{b1} = \sqrt{2}\left(\sqrt{3}-1\right)U_m \sin(\omega t - 7\pi/12) \\ u_{c1} = \sqrt{2}(\sqrt{3}-1)U_m \sin(\omega t + 3\pi/4) \\ u_{a2} = \sqrt{2}\left(\sqrt{3}-1\right)U_m \sin(\omega t - \pi/12) \\ u_{b2} = \sqrt{2}(\sqrt{3}-1)U_m \sin(\omega t - 3\pi/4) \\ u_{c2} = \sqrt{2}(\sqrt{3}-1)U_m \sin(\omega t + 7\pi/12) \end{cases} \tag{19}$$

Furthermore, from the modulation theory, the output voltage of the two three-phase diode-bridge rectifiers can be written as:

$$\begin{cases} u_{d1} = S_{a1}u_{a1} + S_{b1}u_{b1} + S_{c1}u_{c1} \\ u_{d2} = S_{a2}u_{a2} + S_{b2}u_{b2} + S_{c2}u_{c2} \end{cases} \tag{20}$$

where S_{a1}, S_{b1}, S_{c1}, S_{a2}, S_{b2}, and S_{c2} are the switching functions. The switching function S_{a1} can be expressed as:

$$S_{a1} = \begin{cases} 0 & \omega t \in \left[0, \frac{\pi}{12}\right], \omega t \in \left[\frac{9\pi}{12}, \frac{13\pi}{12}\right], \omega t \in \left[\frac{21\pi}{12}, \frac{24\pi}{12}\right] \\ 1 & \omega t \in \left[\frac{\pi}{12}, \frac{9\pi}{12}\right] \\ -1 & \omega t \in \left[\frac{13\pi}{12}, \frac{21\pi}{12}\right] \end{cases} \tag{21}$$

and the relation among the switching functions is:

$$\begin{cases} S_{b1} = S_{a1}\angle - \frac{2\pi}{3} \\ S_{c1} = S_{a1}\angle \frac{2\pi}{3} \end{cases} \qquad \begin{cases} S_{a2} = S_{a1}\angle - \frac{\pi}{6} \\ S_{b2} = S_{b1}\angle - \frac{\pi}{6} \\ S_{c2} = S_{c1}\angle - \frac{\pi}{6} \end{cases} \tag{22}$$

Therefore, the output voltages u_{d1} and u_{d2} can be expressed as:

$$u_{d1} = \begin{cases} (3\sqrt{2}-\sqrt{6})U_m \cos(\omega t + \frac{\pi}{12} - \frac{k\pi}{3}),\ \omega t \in \left[\frac{k\pi}{3}, \frac{k\pi}{3} + \frac{\pi}{12}\right] \\ (3\sqrt{2}-\sqrt{6})U_m \cos(\omega t - \frac{\pi}{4} - \frac{k\pi}{3}), \omega t \in \left[\frac{k\pi}{3} + \frac{\pi}{12}, \frac{(k+1)\pi}{3}\right] \end{cases} \tag{23}$$

$$u_{d2} = \begin{cases} (3\sqrt{2}-\sqrt{6})U_m \cos(\omega t - \frac{\pi}{12} - \frac{k\pi}{3}), \omega t \in \left[\frac{k\pi}{3}, \frac{k\pi}{3} + \frac{\pi}{4}\right] \\ (3\sqrt{2}-\sqrt{6})U_m \cos(\omega t - \frac{5\pi}{12} - \frac{k\pi}{3}), \omega t \in \left[\frac{k\pi}{3} + \frac{\pi}{4}, \frac{(k+1)\pi}{3}\right] \end{cases} \tag{24}$$

From Figure 1, the voltage across the primary winding of the unconventional IPR can be calculated as:

$$u_p = u_{d1} - u_{d2} \tag{25}$$

According to the definition of α_n, the voltage u_s can be expressed as:

$$u_s = \begin{cases} (6-4\sqrt{3})\alpha_n U_m \sin(\omega t - \frac{k\pi}{3}), \omega t \in \left[\frac{k\pi}{3}, \frac{k\pi}{3} + \frac{\pi}{12}\right] \\ (4\sqrt{3}-6)\alpha_n U_m \sin(\omega t - \frac{\pi}{6} - \frac{k\pi}{3}), \omega t \in \left[\frac{k\pi}{3} + \frac{\pi}{12}, \frac{k\pi}{3} + \frac{\pi}{4}\right] \\ (6-4\sqrt{3})\alpha_n U_m \sin(\omega t - \frac{\pi}{3} - \frac{k\pi}{3}), \omega t \in \left[\frac{k\pi}{3} + \frac{\pi}{4}, \frac{(k+1)\pi}{3}\right] \end{cases} \tag{26}$$

From Equation (26), the maximum of the absolute value of u_s is calculated as:

$$|u_s|_{max} = m|u_p|_{max} = \frac{9\sqrt{2}-5\sqrt{6}}{2}\alpha_n U_m \tag{27}$$

Under the operation modes I and II, the unconventional IPR operates as conventional double-tapped IPR and the load voltage u_{d24} can be obtained as:

$$u_{d24} = \begin{cases} \sqrt{3}U_m[\cos(\omega t - \frac{k\pi}{3}) + (4-2\sqrt{3})\alpha_m \sin(\omega t - \frac{k\pi}{3})], \omega t \in [\frac{k\pi}{3}, \frac{k\pi}{3} + \frac{\pi}{12}] \\ \sqrt{3}U_m[\cos(\omega t - \frac{\pi}{6} - \frac{k\pi}{3}) - (4-2\sqrt{3})\alpha_m \sin(\omega t - \frac{\pi}{6} - \frac{k\pi}{3})], \omega t \in [\frac{k\pi}{3} + \frac{\pi}{12}, \frac{k\pi}{3} + \frac{\pi}{6}] \end{cases} \quad (28)$$

from Equation (28), the minimum load voltage is determined by parameter α_m, and can be calculated as:

$$u_{d\ min} = \begin{cases} \frac{\sqrt{2}U_m}{2}[\frac{(3+\sqrt{3})}{2} + (9-5\sqrt{3})\alpha_m], \alpha_m \leq \frac{1}{2(\sqrt{6}-\sqrt{2}+1)} \\ \sqrt{3}U_m, \frac{1}{2(\sqrt{6}-\sqrt{2}+1)} \leq \alpha_m < \frac{1}{2} \end{cases} \quad (29)$$

From Equations (18), (27), and (29), it is obtained that:

$$\begin{cases} \alpha_n - \alpha_m > \frac{4\sqrt{3}+7}{2} = 6.964, \quad \alpha_m \leq \frac{1}{2(\sqrt{6}-\sqrt{2}+1)} \\ \alpha_n > \frac{3\sqrt{6}+5\sqrt{2}}{2} = 7.21, \quad \frac{1}{2(\sqrt{6}-\sqrt{2}+1)} \leq \alpha_m < \frac{1}{2} \end{cases} \quad (30)$$

Therefore, when the parameters α_m and α_n satisfy the above necessary condition, the unconventional IPR can operate normally.

3.3. Optimal Parameters Design

Actually, the above necessary condition is essential and critical but cannot ensure the proposed MPR operating as 36-pulse rectifier. In this section, the optimal turn ratio of the unconventional IPR is designed in order to ensure the proposed MPR operating as 36-pulse rectifier and minimize the input line current THD.

Assume that the first phase angle when the absolute value of u_s is equal to load voltage u_d to be θ, and it meets:

$$u_d(\theta) = |u_s(\theta)| = m|u_p(\theta)| \quad (31)$$

Since the voltage u_s is symmetrical and its period is $\pi/6$, the phase angle θ meets:

$$0 \leq \theta \leq \frac{\pi}{12} \quad (32)$$

From Equations (26), (28), and (31), the resulting equation is:

$$\frac{\sqrt{6}}{2}U_m[\cos(\theta) + (4-2\sqrt{3})\alpha_m \sin(\theta)] = (4\sqrt{3}-6)\alpha_n U_m \sin(\theta) \quad (33)$$

Solving the above equation, the first phase angle θ is:

$$\theta = \arctan\frac{\sqrt{3}}{(4\sqrt{3}-6)(\alpha_n - \alpha_m)} \quad (34)$$

According to the operation mode of unconventional IPR, the output currents of the two three-phase diode-bridge rectifiers can be expressed as follows:

$$i_{d1} = \begin{cases} (0.5-\alpha_m)I_d & \omega t \in [\frac{\pi}{3}k, \frac{\pi}{3}k + \theta] \\ 0 & \omega t \in [\frac{\pi}{3}k + \theta, \frac{\pi}{3}k + \frac{\pi}{6} - \theta] \\ (0.5-\alpha_m)I_d & \omega t \in [\frac{\pi}{3}k + \frac{\pi}{6} - \theta, \frac{\pi}{3}k + \frac{\pi}{6}] \\ (0.5+\alpha_m)I_d & \omega t \in [\frac{\pi}{3}k + \frac{\pi}{6}, \frac{\pi}{3}k + \frac{\pi}{6} + \theta] \\ \frac{\alpha_n I_d}{0.5-\alpha_m+\alpha_n} & \omega t \in [\frac{\pi}{3}k + \frac{\pi}{6} + \theta, \frac{\pi}{3}k + \frac{\pi}{3} - \theta] \\ (0.5+\alpha_m)I_d & \omega t \in [\frac{\pi}{3}k + \frac{\pi}{3} - \theta, \frac{\pi}{3}k + \frac{\pi}{3}] \end{cases} \quad (35)$$

$$i_{\mathrm{d2}} = \begin{cases} (0.5+\alpha_{\mathrm{m}})I_{\mathrm{d}} & \omega t \in [\frac{\pi}{3}k, \frac{\pi}{3}k+\theta] \\ \frac{\alpha_{\mathrm{n}} I_{\mathrm{d}}}{0.5-\alpha_{\mathrm{m}}+\alpha_{\mathrm{n}}} & \omega t \in [\frac{\pi}{3}k+\theta, \frac{\pi}{3}k+\frac{\pi}{6}-\theta] \\ (0.5+\alpha_{\mathrm{m}})I_{\mathrm{d}} & \omega t \in [\frac{\pi}{3}k+\frac{\pi}{6}-\theta, \frac{\pi}{3}k+\frac{\pi}{6}] \\ (0.5-\alpha_{\mathrm{m}})I_{\mathrm{d}} & \omega t \in [\frac{\pi}{3}k+\frac{\pi}{6}, \frac{\pi}{3}k+\frac{\pi}{6}+\theta] \\ 0 & \omega t \in [\frac{\pi}{3}k+\frac{\pi}{6}+\theta, \frac{\pi}{3}k+\frac{\pi}{3}-\theta] \\ (0.5-\alpha_{\mathrm{m}})I_{\mathrm{d}} & \omega t \in [\frac{\pi}{3}k+\frac{\pi}{3}-\theta, \frac{\pi}{3}k+\frac{\pi}{3}] \end{cases} \tag{36}$$

From Figure 1, the input currents of the two three-phase diode bridge rectifiers can be expressed by switching functions as:

$$\begin{cases} i_{\mathrm{a1}} = S_{\mathrm{a1}} i_{\mathrm{d1}} \\ i_{\mathrm{b1}} = S_{\mathrm{b1}} i_{\mathrm{d1}} \\ i_{\mathrm{c1}} = S_{\mathrm{c1}} i_{\mathrm{d1}} \end{cases} \quad \begin{cases} i_{\mathrm{a2}} = S_{\mathrm{a2}} i_{\mathrm{d2}} \\ i_{\mathrm{b2}} = S_{\mathrm{b2}} i_{\mathrm{d2}} \\ i_{\mathrm{c2}} = S_{\mathrm{c2}} i_{\mathrm{d2}} \end{cases} \tag{37}$$

In Figures 1 and 2, according to the Ampere turns balance principle and Kirchoff's current law, it is obtained that:

$$\begin{cases} i_{\mathrm{a}} = 2[\frac{1}{\sqrt{3}}(S_{\mathrm{b1}}-S_{\mathrm{c1}})-S_{\mathrm{b1}}]i_{\mathrm{d1}} + 2[\frac{1}{\sqrt{3}}(S_{\mathrm{c2}}-S_{\mathrm{b2}})-S_{\mathrm{c2}}]i_{\mathrm{d2}} \\ i_{\mathrm{b}} = 2[\frac{1}{\sqrt{3}}(S_{\mathrm{c1}}-S_{\mathrm{a1}})-S_{\mathrm{c1}}]i_{\mathrm{d1}} + 2[\frac{1}{\sqrt{3}}(S_{\mathrm{a2}}-S_{\mathrm{c2}})-S_{\mathrm{a2}}]i_{\mathrm{d2}} \\ i_{\mathrm{c}} = 2[\frac{1}{\sqrt{3}}(S_{\mathrm{a1}}-S_{\mathrm{b1}})-S_{\mathrm{a1}}]i_{\mathrm{d1}} + 2[\frac{1}{\sqrt{3}}(S_{\mathrm{b2}}-S_{\mathrm{a2}})-S_{\mathrm{b2}}]i_{\mathrm{d2}} \end{cases} \tag{38}$$

Substituting Equations (35) and (36) into Equation (38), the input line current i_{a} of the proposed rectifier can be calculated in the time interval of $[0, \pi/2]$:

$$i_{\mathrm{a}} = \begin{cases} (\frac{8\sqrt{3}}{3}-4)\alpha_{\mathrm{m}} I_{\mathrm{d}} & \omega t \in [0,\theta] \\ \frac{(4\sqrt{3}-6)\alpha_{\mathrm{n}}}{3(0.5-\alpha_{\mathrm{m}}+\alpha_{\mathrm{n}})} I_{\mathrm{d}} & \omega t \in [\theta, \frac{\pi}{6}-\theta] \\ [\frac{\sqrt{3}}{3}+(2\sqrt{3}-4)\alpha_{\mathrm{m}}]I_{\mathrm{d}} & \omega t \in [\frac{\pi}{6}-\theta, \frac{\pi}{6}] \\ [\frac{\sqrt{3}}{3}+(4-2\sqrt{3})\alpha_{\mathrm{m}}]I_{\mathrm{d}} & \omega t \in [\frac{\pi}{6}, \frac{\pi}{6}+\theta] \\ \frac{(6-2\sqrt{3})\alpha_{\mathrm{n}}}{3(0.5-\alpha_{\mathrm{m}}+\alpha_{\mathrm{n}})} I_{\mathrm{d}} & \omega t \in [\frac{\pi}{6}+\theta, \frac{\pi}{3}-\theta] \\ [1+(2-\frac{4}{3}\sqrt{3})\alpha_{\mathrm{m}}]I_{\mathrm{d}} & \omega t \in [\frac{\pi}{3}-\theta, \frac{\pi}{3}] \\ [1+(\frac{4}{3}\sqrt{3}-2)\alpha_{\mathrm{m}}]I_{\mathrm{d}} & \omega t \in [\frac{\pi}{3}, \frac{\pi}{3}+\theta] \\ \frac{2\sqrt{3}\alpha_{\mathrm{n}}}{3(0.5-\alpha_{\mathrm{m}}+\alpha_{\mathrm{n}})} I_{\mathrm{d}} & \omega t \in [\frac{\pi}{3}+\theta, \frac{\pi}{2}-\theta] \\ \frac{2\sqrt{3}}{3} I_{\mathrm{d}} & \omega t \in [\frac{\pi}{2}-\theta, \frac{\pi}{2}] \end{cases} \tag{39}$$

In Equation (39), the input line current i_{a} is obviously dependent on the parameters α_{m} and α_{n}. The time interval of $[0, \pi/2]$ is selected because the input line current i_{a} is symmetrical and it is sufficient to determine the THD of input line current. We define the THD of the input line current as:

$$\mathrm{THD} = \frac{\sqrt{{I_{\mathrm{a}}}^2 - {I_1}^2}}{I_1} \tag{40}$$

where I_{a} is the rms value of the input line current i_{a}, I_1 is the rms value of the fundamental of the input line current i_{a}.

From Equation (39), the Fourier series of the input line current i_{a} is calculated as:

$$i_{\mathrm{a}} = \sum_{n=1}^{\infty} \frac{I_{\mathrm{d}}}{n\pi} B_{\mathrm{n}} \sin(n\omega t) \tag{41}$$

where B_{n} meets:

$$B_{\mathrm{n}} = \frac{8\sqrt{3}}{3}\sin\frac{n\pi}{2}\Big\{2(2-\sqrt{3})\alpha_{\mathrm{m}}\sin\frac{n\pi}{3}(2\cos\frac{n\pi}{6}+\sqrt{3}) + \sin n\theta(\cos\frac{n\pi}{3}+\sqrt{3}\cos\frac{n\pi}{6}+1) \\ -(4-2\sqrt{3})\alpha_{\mathrm{m}}[(\sin\frac{n\pi}{6}+\sqrt{3}\sin\frac{n\pi}{3})\cos n\theta + \sin(\frac{n\pi}{2}-n\theta)] + \frac{2\alpha_{\mathrm{n}}\sin(\frac{n\pi}{12}-n\theta)}{0.5+\alpha_{\mathrm{n}}-\alpha_{\mathrm{m}}}(\frac{2\cos\frac{n\pi}{4}}{\sqrt{3}+1}+\frac{\cos\frac{5n\pi}{12}}{2+\sqrt{3}}+\cos\frac{n\pi}{12})\Big\}$$

Furthermore, the rms value of the input line current i_a is calculated as:

$$I_a = \frac{2}{3} I_d \sqrt{[18 + 72(7 - 4\sqrt{3})\alpha_m^2]\frac{\theta}{\pi} + \frac{6(2-\sqrt{3})}{(0.5+\alpha_n-\alpha_m)^2}(1 - \frac{12\theta}{\pi})} \tag{42}$$

and the rms value of the fundamental of the input line current i_a is calculated as:

$$I_1 = \frac{2\sqrt{6}}{3\pi}\left\{\frac{6}{2+\sqrt{3}}[2\alpha_m(1-\cos\theta) + \frac{\alpha_n \cos\theta}{0.5+\alpha_n-\alpha_m}] + \frac{(3-6\alpha_m)\sin\theta}{0.5+\alpha_n-\alpha_m}\right\} \tag{43}$$

Substituting (42) and (43) into (40), the THD of input line current i_a can be obtained. Figure 5 shows the variation in THD of i_a for different parameters α_m and α_n.

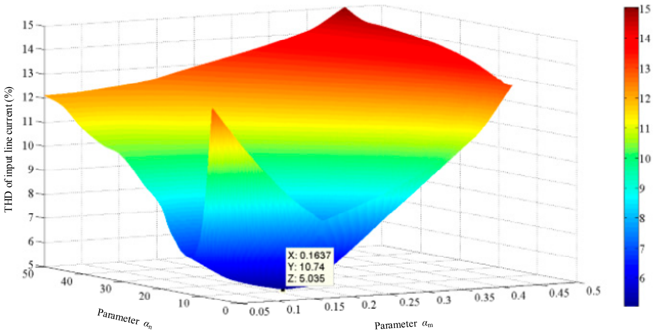

Figure 5. Variation in THD of i_a for different parameter α_m and α_n.

In Figure 5, when the parameter α_m and α_n cannot satisfy the necessary condition, the proposed MPR operates as 24-pulse rectifier and THD of i_a is changing from 7.52% to 15.15% as parameter α_m changes. When the necessary condition is satisfied, the proposed MPR operates as a 36-pulse rectifier and THD of i_a is changing from 5.035% to 7.52% as parameters α_m and α_n change. Especially, when α_m = 0.1637 and α_n = 10.74, the minimum THD of i_a is shown to be 5.035%. Under the optimal parameters, the first phase angle θ is obtained as:

$$\theta = \arctan \frac{\sqrt{3}}{(4\sqrt{3}-6)(\alpha_n - \alpha_m)}\Bigg|_{\substack{\alpha_m = 0.1637 \\ \alpha_n = 10.74}} = \frac{\pi}{18} \tag{44}$$

According to operation mode of the unconventional IPR and substituting the optimal parameters into Equations (35), (36) and (39), we can obtain the waveform of currents i_m, i_n, i_p, i_q i_{d1}, i_{d2} and i_a, as shown in Figure 6.

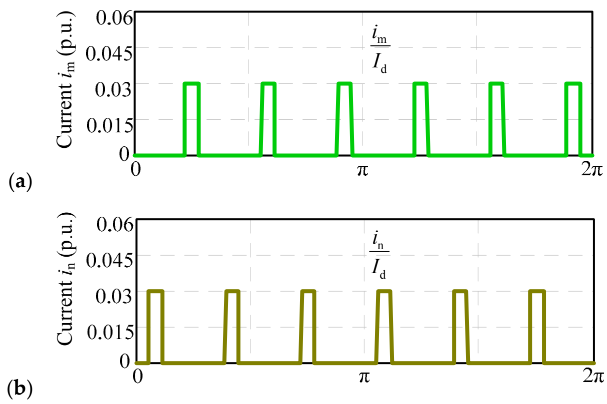

Figure 6. *Cont.*

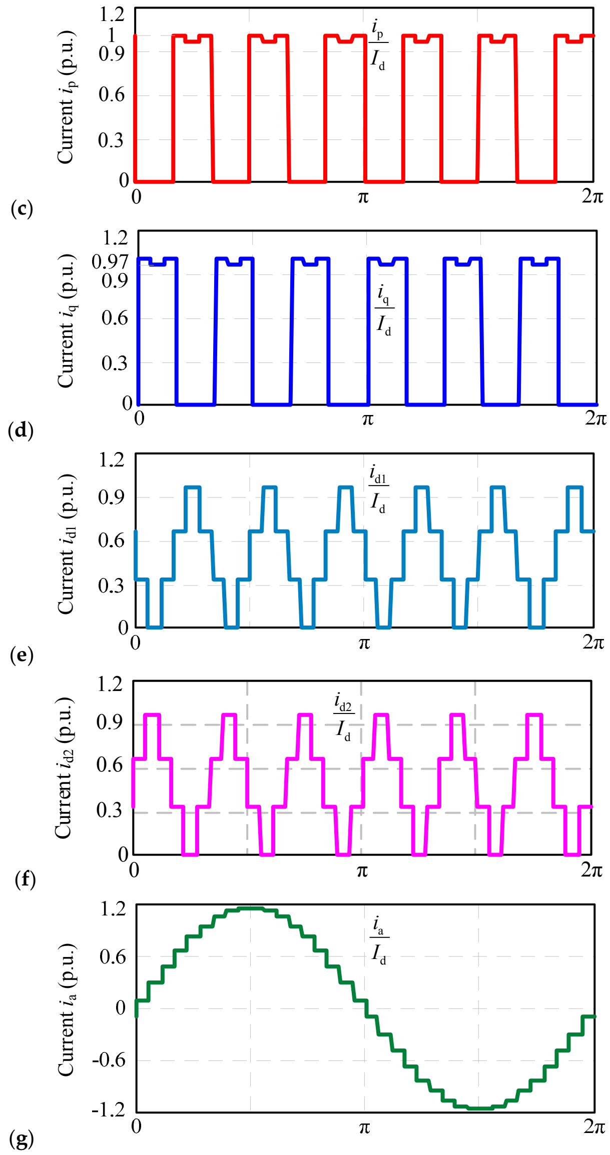

Figure 6. Theoretical currents waveforms. (**a**) Current i_m. (**b**) Current i_n. (**c**) Current i_p. (**d**) Current i_q. (**e**) Current i_{d1}. (**f**) Current i_{d2}. (**g**) Input line current i_a.

Figure 7 shows the spectrum of input line current i_a under the optimal parameters. From Figure 6, the input line current of the proposed rectifier only includes $(36h\pm1)$ *th* (h: integer) harmonics and the proposed rectifier behaves as a 36-pulse rectifier under the optimal parameters.

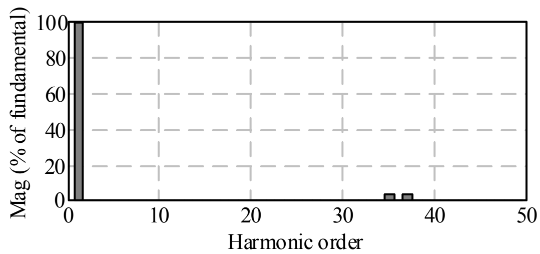

Figure 7. The spectrum of input line current i_a under the optimal parameters.

Actually, there is another way to determine the optimal parameters from the viewpoint of the load voltage. According to the operation mode of the unconventional IPR, the load voltage can be divided into four parts. If the proposed 36-pulse rectifier works normally, the load voltage should have 36 pulses with equal width and equal height per power supply cycle. Therefore, assume that the theoretical waveform of load voltage under the optimal parameters shows as Figure 8. In addition, assume that the first phase angle θ is $\pi/18$.

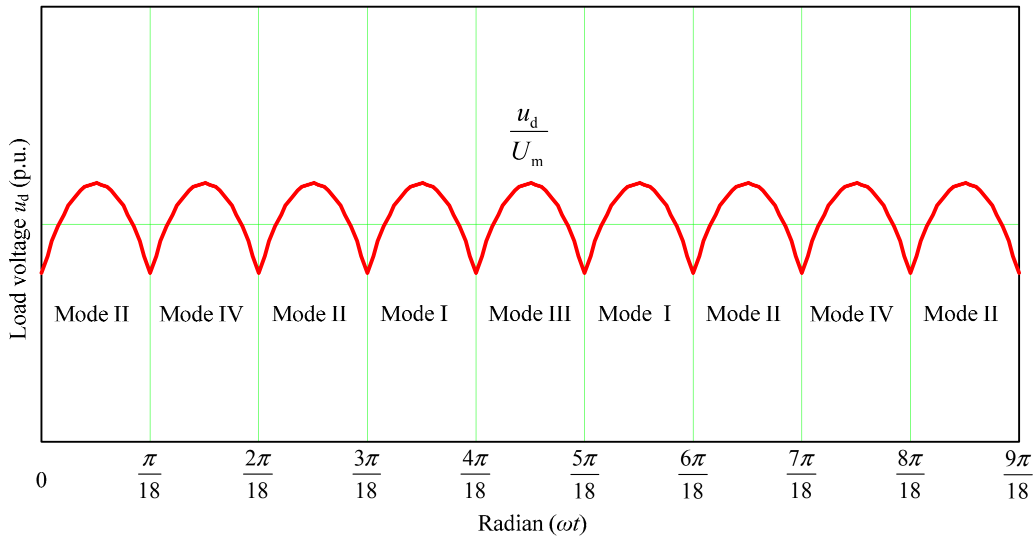

Figure 8. Theoretical waveform of load voltage under the optimal parameters.

From Equation (34), the parameters α_m and α_n satisfy the equation:

$$\alpha_n - \alpha_m = \frac{\sqrt{3}}{(4\sqrt{3} - 6)\tan(\frac{\pi}{18})} \tag{45}$$

In the interval of $[0, \pi/18]$, the unconventional IPR operates under mode II and the load voltage u_d is expressed as Equation (28). This part of the waveform $u_{d\text{-part1}}$ is different when the parameter α_m changes, as Figure 9a shows. The maximum value of Equation (28) can be calculated as:

$$U_{d\text{-part1}} = \sqrt{3 + (84 - 48\sqrt{3})\alpha_m^2}U_m \tag{46}$$

In the interval of $[\pi/18, 2\pi/18]$, the unconventional IPR operates under mode IV. From Equations (17) and (24), the load voltage u_d is expressed as:

$$u_{d\text{-part2}} = \frac{\alpha_n(3\sqrt{2} - \sqrt{6})}{0.5 - \alpha_m + \alpha_n}U_m\cos(\omega t - \frac{\pi}{12}) \tag{47}$$

Furthermore, this part of the waveform $u_{d\text{-part2}}$ is also different when the parameter α_m changes, as Figure 9b shows. The maximum value of the load voltage in this interval can be calculated as:

$$U_{d\text{-part2}} = \frac{\alpha_n(3\sqrt{2} - \sqrt{6})}{0.5 - \alpha_m + \alpha_n}U_m \tag{48}$$

In order to realize the theoretical waveform of load voltage, the Equation (46) should be equal to the Equation (48). From Equations (45), (46) and (48), the parameters α_m and α_n can be calculated as $\alpha_m = 0.1637$ and $\alpha_n = 10.74$. The results are same as the above analysis from the viewpoint of the THD of the input line current.

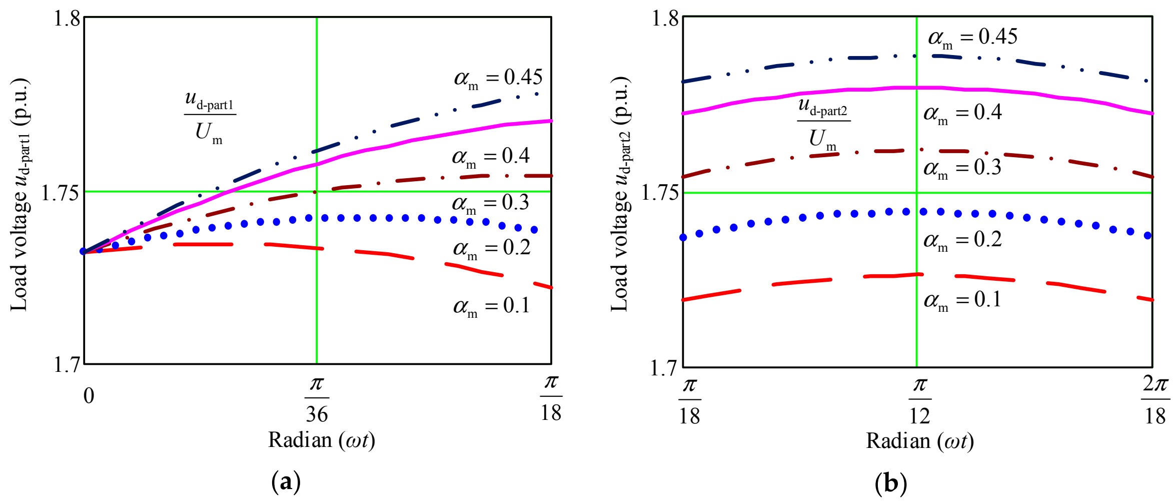

Figure 9. The first part and second part of load voltage waveform with different parameter α_{m}. (**a**) The first part waveform $u_{\text{d-part1}}$; (**b**) The second part waveform $u_{\text{d-part2}}$.

3.4. KVA Rating of the Unconventional IPR

From Figure 3b, according to the MMF relationship, the voltage of the primary winding AT, BT′, and TT′ of the unconventional IPR can be expressed as:

$$u_{\text{AT}} = u_{\text{BT}'} = \frac{1}{2}(1 - 2\alpha_{\text{m}})u_{\text{AB}} \tag{49}$$

$$u_{\text{TT}'} = 2\alpha_{\text{m}} u_{\text{AB}} \tag{50}$$

From Figure 4, after the unconventional IPR is designed optimally, the output voltage of the two-phase diode-bridge rectifiers can be obtained. The voltage across the primary winding of the unconventional IPR can be calculated as:

$$u_{\text{AB}} = \begin{cases} -\sqrt{6-3\sqrt{3}}(\sqrt{6}-\sqrt{2})U_{\text{m}}\sin(\omega t - \frac{\pi}{3}k), \omega t \in [\frac{\pi}{3}k, \frac{\pi}{3}k + \frac{\pi}{18}] \\ -\frac{4\sqrt{6-3\sqrt{3}}}{2(\alpha_{\text{n}}-\alpha_{\text{m}})+1}U_{\text{m}}\cos(\omega t - \frac{\pi}{3}k - \frac{\pi}{12}),\ \omega t \in [\frac{\pi}{3}k + \frac{\pi}{18}, \frac{\pi}{3}k + \frac{\pi}{9}] \\ \sqrt{6-3\sqrt{3}}(\sqrt{6}-\sqrt{2})U_{\text{m}}\sin(\omega t - \frac{\pi}{3}k - \frac{\pi}{6}), \omega t \in [\frac{\pi}{3}k + \frac{\pi}{9}, \frac{\pi}{3}k + \frac{\pi}{6}] \\ \sqrt{6-3\sqrt{3}}(\sqrt{6}-\sqrt{2})U_{\text{m}}\sin(\omega t - \frac{\pi}{3}k - \frac{\pi}{6}), \omega t \in [\frac{\pi}{3}k + \frac{\pi}{6}, \frac{\pi}{3}k + \frac{2\pi}{9}] \\ \frac{4\sqrt{6-3\sqrt{3}}}{2(\alpha_{\text{n}}-\alpha_{\text{m}})+1}U_{\text{m}}\cos(\omega t - \frac{\pi}{3}k - \frac{\pi}{4}),\ \omega t \in [\frac{\pi}{3}k + \frac{2\pi}{9}, \frac{\pi}{3}k + \frac{5\pi}{18}] \\ -\sqrt{6-3\sqrt{3}}(\sqrt{6}-\sqrt{2})U_{\text{m}}\sin(\omega t - \frac{\pi}{3}k - \frac{\pi}{3}), \omega t \in [\frac{\pi}{3}k + \frac{5\pi}{18}, \frac{\pi}{3}k + \frac{\pi}{3}] \end{cases} \tag{51}$$

From Equation (51), the rms value of the u_{AB} under the optimal parameters is calculated as:

$$U_{\text{AB}} \approx 0.1205 U_{\text{m}} \tag{52}$$

The rms value of the voltage across the secondary winding can be expressed as:

$$U_{\text{s}} = \alpha_{\text{n}} U_{\text{AB}} \approx 1.2941 U_{\text{m}} \tag{53}$$

From Equations (35) and (36), according to the operation mode of the unconventional IPR, the rms value of the current through the primary winding AT or BT′ of the IPR can be calculated as:

$$I_{\text{d1}} = I_{\text{d2}} = 0.5836 I_{\text{d}} \tag{54}$$

The rms value of the current through the primary winding TT′ of the IPR can be calculated as:

$$I_{\mathrm{TT'}} = 0.2753 I_{\mathrm{d}} \tag{55}$$

Furthermore, the rms value of current through the secondary winding of IPR can be calculated as:

$$I_{\mathrm{m}} = I_{\mathrm{n}} = 0.0124 I_{\mathrm{d}} \tag{56}$$

Therefore, the kVA rating of the unconventional IPR is calculated as:

$$S_{\mathrm{UIPR}} = 0.5(U_{\mathrm{AT}} I_{\mathrm{d1}} + U_{\mathrm{BT}} I_{\mathrm{d2}} + U_{\mathrm{TT'}} I_{\mathrm{TT'}} + U_{\mathrm{s}} I_{\mathrm{m}} + U_{\mathrm{s}} I_{\mathrm{n}}) \approx 2.60\% U_{\mathrm{d}} I_{\mathrm{d}} \tag{57}$$

3.5. KVA Rating of the ZSBT

As discussed in [5], the voltage across the ZSBT is expressed as:

$$u_{\mathrm{ZSBT}} = \begin{cases} \frac{(\sqrt{6}-\sqrt{2})^2}{2} U_{\mathrm{m}} \cos(\omega t - \frac{2\pi}{3}k - \frac{2\pi}{3}) \omega t \in [\frac{2\pi}{3}k, \frac{2\pi}{3}k + \frac{7\pi}{18}] \\ (\sqrt{6}-\sqrt{2}) U_{\mathrm{m}} [\frac{\sqrt{6}+\sqrt{2}}{2} \cos(\omega t - \frac{2\pi}{3}k - \frac{\pi}{3}) - \frac{2(\alpha_{\mathrm{n}}-\alpha_{\mathrm{m}})-1}{2(\alpha_{\mathrm{n}}+\alpha_{\mathrm{m}})+1} \sqrt{3} \cos(\omega t - \frac{2\pi}{3}k - \frac{5\pi}{12})] \\ \quad \omega t \in [\frac{2\pi}{3}k + \frac{7\pi}{18}, \frac{2\pi}{3}k + \frac{4\pi}{9}] \\ \sqrt{2}(\sqrt{6}-\sqrt{2}) U_{\mathrm{m}} \cos(\omega t - \frac{2\pi}{3}k) \omega t \in [\frac{2\pi}{3}k + \frac{4\pi}{9}, \frac{2\pi}{3}k + \frac{5\pi}{9}] \\ (\sqrt{6}-\sqrt{2}) U_{\mathrm{m}} [\frac{\sqrt{6}+\sqrt{2}}{2} \cos(\omega t - \frac{2\pi}{3}k + \frac{\pi}{3}) + \frac{2(\alpha_{\mathrm{n}}-\alpha_{\mathrm{m}})-1}{2(\alpha_{\mathrm{n}}+\alpha_{\mathrm{m}})+1} \sqrt{3} \cos(\omega t - \frac{2\pi}{3}k - \frac{7\pi}{12})] \\ \quad \omega t \in [\frac{2\pi}{3}k + \frac{5\pi}{9}, \frac{2\pi}{3}k + \frac{11\pi}{18}] \\ \frac{(\sqrt{6}-\sqrt{2})^2}{2} U_{\mathrm{m}} \cos(\omega t - \frac{2\pi}{3}k + \frac{2\pi}{3}) \omega t \in [\frac{2\pi}{3}k + \frac{11\pi}{18}, \frac{2\pi}{3}k + \frac{2\pi}{3}] \end{cases}, \tag{58}$$

Furthermore, the rms value of voltage across the ZSBT is calculated as:

$$U_{\mathrm{ZSBT}} = \sqrt{\frac{1}{T} \int_0^T u_{ZSBT}^2 \mathrm{d}\omega t} \approx 0.1249 U_{\mathrm{d}}, \tag{59}$$

Therefore, according to Equations (54) and (59), the kVA rating of the ZSBT is calculated as:

$$S_{\mathrm{ZSBT}} = 0.5[U_{\mathrm{ZSBT}}(I_{\mathrm{d1}} + I_{\mathrm{d2}})] \approx 7.29\% U_{\mathrm{d}} I_{\mathrm{d}}, \tag{60}$$

4. Experimental Results

In order to validate the theoretical analysis, an experimental setup with 3 kW is designed. Table 1 shows the rectifier specifications and components.

Table 1. Rectifier specifications and components for experiments.

Parameter	Value
Input phase voltage (rms)	120 V
Line frequency	50 Hz
Load filtering inductance	10 mH
Primary tapped ratio (α_{m}) of the unconventional IPR	0.16
Turn ratio (α_{n}) of the unconventional IPR	10.74
Rated output power	3 kW
Rated output current	10 A

The input rectifier is from a programmable 61511 AC source (Chroma, Bellows Falls, VT, USA) and the power quality analyzer is a HIOKI 3196 (HIOKI, Ueda, Nagano, Japan).

Under the rated conditions listed in Table 1, Figure 10a shows the input line currents and their THD when the unconventional IPR operating as double-tapped IPR. The proposed rectifier behaves as a 24-pulse rectifier and the input line current THD is about 6.5% which is slightly less than the theoretical value. Because the tapped ratio $\alpha_m = 0.16$ is not the optimal parameter for 24-pulse rectifier with double-tapped IPR, there are also 11th and 13th harmonic components in the spectrum of the input line current.

Figure 10b shows the input line currents and their THD when the unconventional IPR has the optimal parameters. The proposed rectifier behaves as a 36-pulse rectifier and the experimental value of THD is about 4.3%. Whether the unconventional IPR operates as a double-tapped IPR or under optimal condition, the experimental value of THD is less than that of the theoretical value due to the filtering effect of leakage inductance of autotransformer and inductance of IPR and ZSBT. Compared with Figure 10a, the unconventional IPR is effective on reducing harmonic distortion of the rectifier input currents.

Figure 11 shows the measured waveforms. Figure 11a shows the primary diodes currents i_p and i_q of the unconventional IPR. Figure 11b shows the secondary diodes currents i_m and i_n of the unconventional IPR, and the output current i_f of SFR. Compared with the primary diodes currents, the secondary diodes currents are very small. Figure 11c shows the output currents i_{d1} and i_{d2} of the two three-phase diode-bridge rectifier. The currents i_{d1} and i_{d2} are modulated obviously when the unconventional IPR with optimal parameters. The waveforms of these currents basically coincide with the theoretical analysis in Figure 6. Figure 11d shows the input currents i_{a1} and i_{b1} of the three-phase diode-bridge rectifier I (REC I in Figure 1). Figure 11e shows the output voltages u_{d1} and u_{d2} of the two three-phase diode-bridge rectifier. Figure 11f shows the load voltage, which are smothered in the experimental results due to the load filtering inductance.

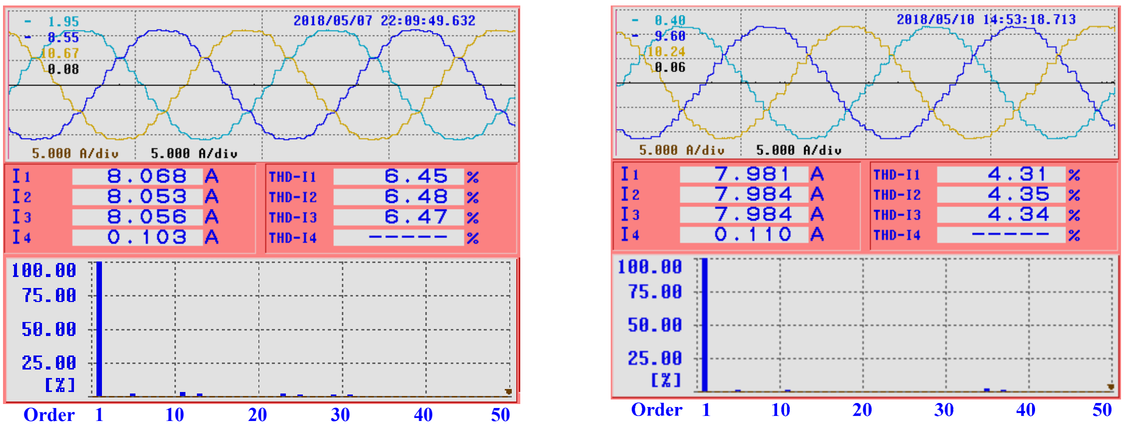

(**a**) (**b**)

Figure 10. Input line currents and their spectrums. (**a**) When the unconventional IPR operating as double-tapped IPR. (**b**) When the unconventional IPR with the optimal parameters.

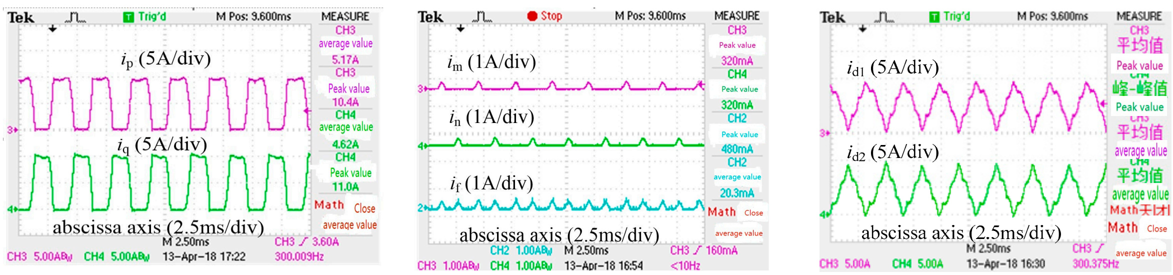

(**a**) (**b**) (**c**)

Figure 11. *Cont.*

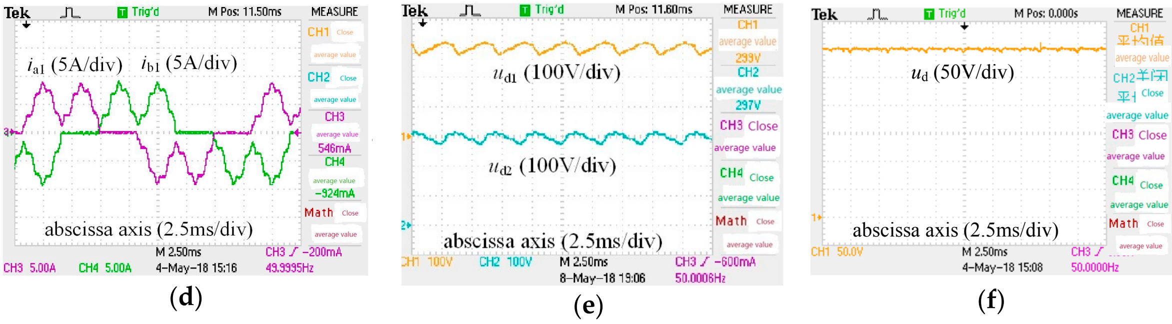

Figure 11. Measured waveforms of the proposed rectifier. (**a**) Currents i_p and i_q of diodes D_p and D_q. (**b**) Currents i_m and i_n of diodes D_m and D_n, and output current i_f of SFR. (**c**) Output currents i_{d1} and i_{d2} of the two three-phase diode-bridge rectifier. (**d**) Input currents i_{a1} and i_{b1} of the three-phase diode-bridge rectifier I. (**e**) Output voltages u_{d1} and u_{d2} of the two three-phase diode-bridge rectifier. (**f**)Load voltage.

Figure 12 shows the waveforms of input line currents of MPRs under the rated conditions listed in Table 1. Table 2 shows the comparison of input line current THD, IPR kVA rating, load power and efficiency.

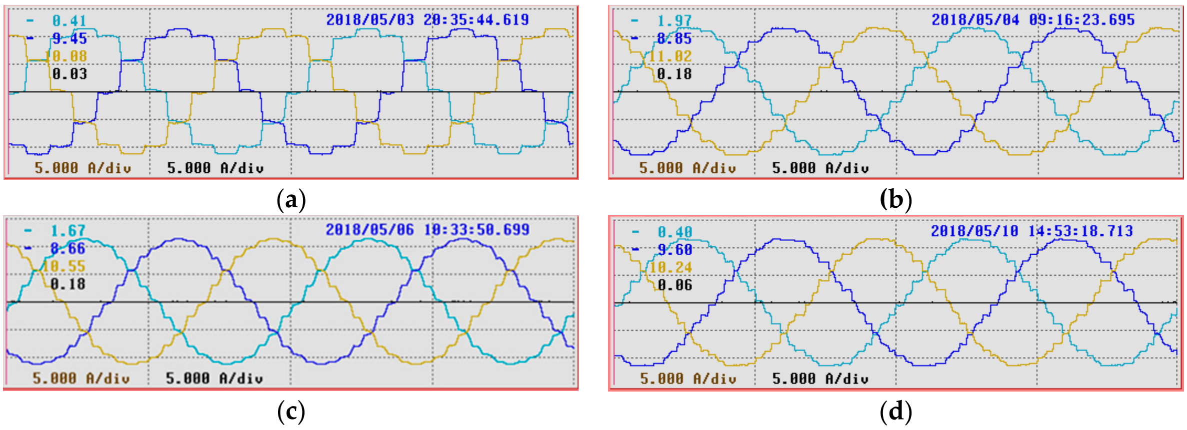

Figure 12. Waveforms of input line currents. (**a**) Conventional 12-pulse rectifier. (**b**) 24-pulse rectifier with double-tapped IPR. (**c**) 24-pulse rectifier with unconventional IPR. (**d**) Proposed 36-pulse rectifier with unconventional IPR.

Table 2. Comparison of the Proposed Rectifier with Other MPRs.

Topologies	Input line Current THD	IPR kVA Rating	Load Power	Efficiency
12-pulse rectifier with conventional IPR	12.23%	2.04% U_dI_d	2932.1 W	96%
24-pulse rectifier with double-tapped IPR	5.93%	1.65% U_dI_d	2941.2 W	96.3%
24-pulse rectifier with unconventional IPR	5.62%	3.11% U_dI_d	2944.3 W	96.4%
36-pulse rectifier with unconventional IPR	4.34%	2.60% U_dI_d	2965.6 W	97.1%

From Figure 12a, the input line current of conventional 12-pulse rectifier contains 12 steps with equal width per power supply cycle and the experimental THD is about 12.23%. Figure 12b shows the input line current of 24-pulse rectifier with double-tapped IPR. Compared with Figure 11a, the experimental THD is small because the double-tapped IPR is designed optimally. Figure 12c shows the input line current of 24-pulse rectifier with unconventional IPR designed optimally according to [19]. From Figure 12b,c, the step number of input line currents of both 24-pulse rectifiers is increased from 12 to 24. From Figure 12d, the input line current of proposed 36-pulse rectifier contains 36 steps with equal width per power supply cycle when the unconventional IPR designed optimally. From Table 2, the experimental THD of input line current is decreased as the pulse number of load voltage and the step number of input line current increasing. Though the IPR kVA rating in 24-pulse rectifier with double-tapped IPR is small, the kVA rating of other magnetic components will increase. From the experiment results, the efficiency of proposed 36-pulse rectifier with unconventional IPR is slightly improved.

5. Conclusions

This paper proposes an unconventional IPR to extend the conventional 24-pulse diode rectifier with double-tapped IPR to a 36-pulse rectifier. The primary winding of the unconventional IPR is double-tapped and the secondary winding is connected with SFR. When the unconventional IPR is designed optimally, under ideal conditions, the proposed rectifier operates as a 36-pulse rectifier and draws near sinusoidal input line currents. The operation mode, the optimal parameters and kVA rating of the unconventional IPR are analyzed and derived in this paper. Under optimal parameter conditions, the THD of input line currents is about 5.035% and the current through the secondary winding of the unconventional IPR is very small. Above all, compared with the conventional 36-pulse rectifier using the three-tapped IPR, the proposed rectifier is easy to realize instead of control circuit.

Author Contributions: Under the supervision of S.Y., Y.L. carried out this research work. S.Y. proposed the main idea and analysis method. Y.L. was responsible for the theoretical derivation and manuscript writing. H.B. proposed suggestions and right directions to design the experimental work. W.Y. carried out the simulation and helped Y.L. to perform the experiments.

Funding: This work was supported by National Natural Science Foundation of China (Grant No.51677036).

Conflicts of Interest: The authors declare no conflict of interest.

References

1. Rodriguez, J.; Pontt, J.; Silva, C.; Wiechmann, E.; Hammond, P.; Santucci, F.W.; Álvarez, R.; Musalem, R.; Kouro, S.; Lezana, P. Large current rectifiers: State of the art and future trends. *IEEE Trans. Ind. Electron.* **2005**, *52*, 738–746. [CrossRef]
2. Singh, B.; Gairola, S.; Singh, B.; Chandra, A.; Al-Haddad, K. Multipulse AC-DC converters for improving power quality: A review. *IEEE Trans. Power Electron.* **2008**, *23*, 260–281. [CrossRef]
3. Das, J. *Harmonic Reduction at the Source*; IEEE Press: New York, NY, USA, 2015.
4. Prakash, P.S.; Kalpana, R.; Singh, B.; Bhuvaneswari, G. A 20-pulse asymmetric multiphase staggering autoconfigured transformer for power quality improvement. *IEEE Trans. Power Electron.* **2018**, *33*, 917–925.
5. Choi, S.; Lee, B.; Enjeti, P. New 24-pulse diode rectifier systems for utility interface of high-power AC motor drives. *IEEE Trans. Ind. Appl.* **1997**, *33*, 531–541. [CrossRef]
6. Abdollahi, R.; Gharehpetian, G. Inclusive design and implementation of novel 40-pulse ac-dc converter for retrofit application and harmonic mitigation. *IEEE Trans. Ind. Electron.* **2016**, *63*, 667–677. [CrossRef]
7. Khan, S.; Zhang, X.; Saad, M.; Ali, H.; Khan, B.; Zaman, H. Comparative analysis of 18-pulse autotransformer rectifier unit topologies with intrinsic harmonic current cancellation. *Energies* **2018**, *11*, 1347. [CrossRef]
8. Singh, B.; Bhuvaneswari, G.; Garg, V. T-connected autotransformerbased 24-pulse AC–DC converter for variable frequency induction motor drive. *IEEE Trans. Energy Convers.* **2006**, *21*, 663–672. [CrossRef]
9. Mon-Nzongo, D.L.; Ipoum-Ngome, P.G.; Jin, T.; Song-Manguelle, J. An improved topology for multipulse AC/DC converters within HVDC and VFD systems: Operation in degraded Modes. *IEEE Trans. Ind. Electron.* **2018**, *65*, 3646–3656. [CrossRef]
10. Yang, T.; Bozhko, S.; Asher, G. Functional modeling of symmetrical multipulse autotransformer rectifier units for aerospace applications. *IEEE Trans. Power Electron.* **2015**, *30*, 4704–4713. [CrossRef]

11. Singh, B.; Bhuvaneswari, G.; Kalpana, R. Autoconnected transformer based 18-pulse ac-dc converter for power quality improvement in switched mode power supplies. *IEEE Trans. Power Electron.* **2010**, *3*, 525–541. [CrossRef]
12. Meng, F.; Yang, W.; Zhu, Y.; Gao, L.; Yang, S. Load adaptability of active harmonic reduction for 12-pulse diode bridge rectifier with active interphase reactor. *IEEE Trans. Power Electron.* **2015**, *30*, 7170–7180. [CrossRef]
13. Biela, J.; Hassler, D.; Schönberger, J.; Kolar, J.W. Closed-loop sinusoidal input-current shaping of 12-pulse autotransformer rectifier unit with impressed output voltage. *IEEE Trans. Power Electron.* **2011**, *26*, 249–259. [CrossRef]
14. Sandoval, J.J.; Krishnamoorthy, H.S.; Pitel, I. Reduced active switch front-end multipulse rectifier with medium-frequency transformer isolation. *IEEE Trans. Power Electron.* **2017**, *32*, 7458–7468. [CrossRef]
15. Young, C.; Chen, M.; Lai, C.; Shih, D. A novel active interphase transformer scheme to achieve three-phase line current balance for 24-pulse converter. *IEEE Trans. Power Electron.* **2012**, *27*, 1719–1731. [CrossRef]
16. Pan, Q.; Ma, W.; Liu, D.; Zhao, Z.; Meng, J. A new critical formula and mathematical model of double-tap interphase reactor in a six-phase tap-changer diode rectifier. *IEEE Trans. Ind. Electron.* **2007**, *54*, 479–485.
17. Meng, F.; Yang, S.; Yang, W. Modeling for a multitap interphase reactor in a multipulse diode bridge rectifier. *IEEE Trans. Power Electron.* **2009**, *24*, 2171–2177. [CrossRef]
18. Singh, B.; Garg, V.; Bhuvaneswari, G. Polygon-connected autotransformer-based 24-pulse AC–DC converter for vector-controlled induction-motor drives. *IEEE Trans. Ind. Electron.* **2008**, *55*, 197–208. [CrossRef]
19. Yang, S.; Wang, J.; Yang, W. A Novel 24-Pulse Diode Rectifier with an Auxiliary Single-Phase Full-Wave Rectifier at DC Side. *IEEE Trans. Power Electron.* **2017**, *32*, 1885–1893. [CrossRef]
20. Chivite-Zabalza, F.J.; Forsyth, A.J.; Araujo-Vargas, I. 36-Pulse Hybrid Ripple Injection for High-Performance Aerospace Rectifiers. *IEEE Trans. Ind. Appl.* **2009**, *45*, 992–999. [CrossRef]
21. Li, X.; Xu, W.; Ding, T. Damped high passive filter—A new filtering scheme for multipulse rectifier systems. *IEEE Trans. Power Deliv.* **2017**, *32*, 117–124. [CrossRef]
22. Paice, D.A. *Power Electronic Converter Harmonic Multipulse Methods for Clean Power*; IEEE Press: New York, NY, USA, 1996.
23. Meng, F.; Gao, L.; Yang, S.; Yang, W. Effect of phase-shift angle on a delta-connected autotransformer applied to a 12-pulse rectifier. *IEEE Trans. Ind. Electron.* **2015**, *62*, 4678–4690. [CrossRef]
24. Meng, F.; Yang, W.; Yang, S. Effect of voltage transformation ratio on the kilovoltampere rating of delta-connected autotransformer for 12-pulse rectifier system. *IEEE Trans. Ind. Electron.* **2013**, *60*, 3579–3588. [CrossRef]